Pergamon

Int. J. Heat Mass Transfer. Vol. 38, No. 15, pp. 2863–2871, 1995

0017–9310/95 $9.50+0.00

0017–9310(95)00001–1

The mechanism of heat transfer enhancement for mineral oil in 2 : 1 rectangular ducts

F. C. CHOU and C. W. TUNG
Department of Mechanical Engineering, National Central University, Chung-Li, 320 Taiwan, Republic of China

(*Received* 13 *June* 1994 *and in final form* 9 *November* 1994)

Abstract—A numerical study is performed to study the mechanism of heat transfer enhancement for mineral oil in 2 : 1 rectangular ducts. Three different heating conditions are considered: top wall heated, bottom wall heated, and both top and bottom walls heated. For the three heating conditions, the present numerical results are all in good agreement with the experimental data. For the case of top wall heated, the heat transfer enhancement is caused mainly by the axial velocity distortion due to temperature dependence of viscosity. For the case of bottom wall heated, the axial velocity distortion is the major factor to heat transfer enhancement in the region near the entrance. While near the fully-developed region, the heat transfer enhancement is mainly caused by the buoyancy-induced secondary flow. The mechanism of heat transfer enhancement for the case of top and bottom walls heated is more like that for bottom wall heated.

INTRODUCTION

This study stems from the practical requirement of high heat transfer enhancement in the design of modern compact heat exchangers in general and liquid cooling for electronic modules. It is known that the heat transfer coefficients for laminar flow depend on the tube geometry, heating condition, fluid properties, temperature dependence of fluid properties, flow rate, axial location, usage of enhancement device or insertion, and so on. Recently, significant heat transfer enhancements were reported by Hartnett and his coworkers [1–4] for mineral oil or non-Newtonian fluids in a 2 : 1 rectangular channel. Though the surprising results of heat transfer enhancement were reported, the understanding of the mechanism of heat transfer enhancement for the fluids with temperature-dependent viscosity is still limited.

There are a number of studies on the influence of temperature-dependent viscosity on internal flow heat transfer. Sieder and Tate [5] and Deissler [6] were the early experimental and analytical studies of the effect of variable viscosity on laminar heat transfer in the fully-developed region of circular tube. Analytical solutions for laminar forced convection in both the developing and fully developed region of circular tube were reported by Yang [7] and Test [8]. Analytical studies of fully-developed laminar heat transfer with the combined effect of variable viscosity and free convection were reported by Shannon and Depew [9] and Hong and Bergles [10]. Oskay and Kakac [11] investigated the heat transfer of mineral oil flowing through a circular pipe with constant heat flux. Butler and Mckee [12] worked out an exact solution of velocity distribution for fully developed flow of temperature-dependent viscous fluids in heated rectangular ducts.

From the foregoing paper review, it is found that most earlier works are focused on the flows in circular tube. But in the past few years, the study of flow and heat transfer behavior in rectangular channels has become increasingly important due to the significant heat transfer enhancement, which was not observed in a circular tube flow. Xie and Hartnett [1] experimentally studied the laminar heat transfer of mineral oil in a 2 : 1 rectangular channel. Three different heating configurations were used: top wall heated, bottom wall heated, and top and bottom walls heated. Shin *et al.* [13] reported a numerical study of laminar heat transfer for temperature-dependent viscosity fluids in a 2 : 1 rectangular channel. It is worthy to note that only top wall heated configuration was considered and free convection effect was neglected. Chou *et al.* [14] showed a numerical study of non-Newtonian flow and heat transfer enhancement in an asymmetrically heated parallel plate channel. There is still no thorough study of mechanism of heat transfer enhancement for mineral oil in the rectangular duct with the three heating configurations.

THEORETICAL ANALYSIS

Consider a steady three-dimensional laminar flow in the entrance region of a horizontal 2 : 1 rectangular channel as shown in Fig. 1. The channel is adiabatic at the side walls, and three different heating conditions are considered: top wall heated, bottom wall heated, and both top and bottom walls heated. The Prandtl number of mineral oil is 511.5 at 20°C [13]. The growth of momentum boundary layer is much faster

NOMENCLATURE

A cross-sectional area of a channel
b viscosity variation parameter defined by equation (1)
C a constant, $-(D_h/\mu W_0)\partial P_f/\partial Z$
D_h equivalent hydraulic diameter, $4A/S$
Gr_q Grashof number, $g\beta\theta_c D_h{}^3/v^2$
g acceleration due to gravity
h average heat transfer coefficient
k thermal conductivity
M, N number of divisions in x and y directions, respectively
Nu local Nusselt number, $\bar{h}D_h/k$
n outward normal direction to the wall
P, P_f pressure deviation and pressure for fully developed laminar flow before thermal entrance, respectively
Pe Peclet number, $RePr$
Pr Prandtl number, v/α
Q dimensionless parameter for a measure of temperature dependence for viscosity, bq_wD_h/k
q_w uniform heat flux
Ra_q Rayleigh number, $PrGr_q$
Re Reynolds number, W_0D_h/v
S circumference of cross-section
T temperature
T_{ref} reference temperature
U, V, W velocity components in X, Y and Z directions
u, v, w dimensionless quantity for U, V and W, respectively
W_f Fully developed axial velocity before thermal entrance
W_0 average value of axial velocity over the cross-section
X, Y, Z rectangular coordinates
x, y, z dimensionless rectangular coordinates.

Greek symbols
α thermal diffusively
β coefficient of thermal expansion with temperature
θ dimensionless temperature, $(T-T_{ref})/\theta_c$
θ_c characteristic temperature, q_wD_h/k
$\mu, \bar{\mu}$ dynamic viscosity and its dimensionless quantity
$v, \bar{v}$ kinematic viscosity and its dimensionless quantity
ξ vorticity in the axial direction, $\partial u/\partial y - \partial v/\partial x$
ρ density.

Subscripts
b bulk mean value
c characteristic quantity
ref reference state
w value at wall.

than that of thermal boundary layer, therefore it is reasonable to assume a fully developed velocity profile imposed at the entrance of heating section. For most high viscosity liquids, although the values of specific heat and thermal conductivity are rather insensitive to temperature, the viscosity decreases significantly with the increase of temperature. The viscosity model is described by an exponential model

$$\mu = \mu_{ref} \exp[-b(T-T_{ref})] \tag{1}$$

or in dimensionless form

$$\bar{\mu} = \mu/\mu_{ref} = \exp(-Q\theta) \tag{2}$$

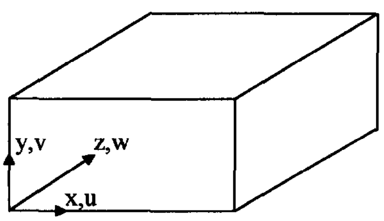

Fig. 1. Schematic for numerical solution and the coordinate system.

where b is a viscosity variation parameter, $\theta = (T-T_{ref})/\theta_c$ is a dimensionless temperature, $\theta_c = q_wD_h/k$ is the characteristic temperature, $Q = b(q_wD_h/k)$ is a measure of magnitude of temperature dependence for viscosity and μ_{ref} is the reference viscosity at T_{ref}. The Boussinesq approximation is used to characterize the buoyancy effect. The viscous dissipation and compression effects are neglected. The dimensionless variables and parameters are introduced:

$$x = X/D_h, \quad y = Y/D_h, \quad z = Z/(PrReD_h),$$
$$u = U/U_0, \quad v = V/U_0, \quad w = W/W_0,$$
$$p = P/(\rho W_0 v/D_h), \quad Gr_q = g\beta\theta_c D_h^3/v^2, \quad Pr = v/\alpha,$$
$$Ra_q = PrGr_q, \quad Re = W_0D_h/v, \quad Pe = PrRe \tag{3}$$

where $D_h = 4A/S$, $U_0 = Gr_q v/D_h$ and W_0 is the mean value of axial velocity W over the cross section. By introducing a vorticity function in the axial direction, $\xi = \partial u/\partial y - \partial v/\partial x$, the vorticity–velocity formulation of Navier–Stokes equations can be derived and shown as follows:

$$\nabla^2 u = \partial\xi/\partial y - \partial w/\partial x\,\partial z \quad (4)$$

$$\nabla^2 v = -\partial\xi/\partial x - \partial w/\partial y\,\partial z \quad (5)$$

$$\begin{aligned} &Gr_q(u\,\partial\xi/\partial x + v\,\partial\xi/\partial y + \xi\,\partial u/\partial x + \xi\,\partial v/\partial y) \\ &\quad + [(\partial w/\partial y)(\partial u/\partial z) - (\partial w/\partial x)(\partial v/\partial z) + w\,\partial\xi/\partial z]/Pr \\ &= \bar{v}\nabla^2\xi + 2(\partial v/\partial y)\nabla^2 u - 2(\partial v/\partial x)\nabla^2 v \\ &\quad + (\partial^2 v/\partial y^2 - \partial^2 v/\partial x^2)(\partial u/\partial y + \partial v/\partial x) \\ &\quad + 2(\partial^2 v/\partial x\,\partial y)(\partial u/\partial x - \partial v/\partial y) + (\partial\theta/\partial x) \quad (6) \end{aligned}$$

$$\begin{aligned} &Gr_q(u\,\partial w/\partial x + v\,\partial w/\partial y) + (w\,\partial w/\partial z)/Pr \\ &= -(\partial p/\partial z)/Pe + \bar{v}\nabla^2 w + (\partial w/\partial x)(\partial v/\partial x) \\ &\quad + (\partial w/\partial y)(\partial v/\partial y) \quad (7) \end{aligned}$$

$$\nabla^2 w = C \quad (8)$$

$$Ra_q(u\,\partial\theta/\partial x + v\,\partial\theta/\partial y) + w\,\partial\theta/\partial z = \nabla^2\theta \quad (9)$$

where $\nabla^2 = (\partial^2/\partial x^2 + \partial^2/\partial y^2)$ and $C = -(D_h/\mu W_0) \times \partial P_f/\partial Z$ = constant. It should be noted that the axial diffusion terms in equations (6), (7) and (9) are neglected under the condition of high Peclet number for the oil flow in the experimental work of Xie and Hartnett [1].

Because of the geometrical symmetry in rectangular duct, it suffices to consider one half of the duct. Therefore, the boundary conditions are as follows:

$$\begin{aligned} &u = v = w = 0 && \text{at all walls} \\ &\partial\theta/\partial n = 1 && \text{at heated walls} \\ &\partial\theta/\partial n = 0 && \text{at adiabatic walls} \\ &u = \partial v/\partial x = \partial w/\partial x = \partial\theta/\partial x = 0 && \\ & && \text{at the plane of symmetry.} \quad (10) \end{aligned}$$

After the developing velocity profile and temperature fields along the axial direction are obtained, the computation of local Nusselt number is of interest. The local Nusselt number Nu along the heated walls is defined as

$$Nu = \bar{h}D_h/k = 1/(\bar{\theta}_w - \theta_b) \quad (11)$$

where $\bar{\theta}_w$ is the averaged temperature at the heated wall and θ_b is the fluid bulk mean temperature. Simpson's rule is used to compute the average quantities indicated above.

Though the governing equations (4)–(9) are more complicated than those shown in Chou and Hwang [15], the computation procedure for the simultaneous solutions of equations (4)–(9) with boundary conditions (10) is the same in principle.

RESULTS AND DISCUSSION

Numerical experiments were carried out to ensure the accuracy of the present results. First, the values of bulk mean temperature θ_b were checked by the known analytical results $\theta_b = 4z/3$ for the cases of top wall heated or bottom wall heated and $\theta_b = 8z/3$ for the case of both top and bottom walls heated. The above-mentioned analytical results may be obtained by considering an overall energy balance for a dimensionless axial length dz. The deviations were seen to be less than 1.5%. Second, the values of Nusselt number should be independent of the axial step size Δz and $M \times N$, which is the number of divisions in x and y directions of the computation domain. The local Nusselt number Nu, which are calculated by using $M \times N = 48 \times 48$, 60×60 and 80×80 and $\Delta z = 5 \times 10^{-6}$ and 2×10^{-6}, are shown in Table 1 for the case of $Q = 18.72$, $Ra_q = 19.7 \times 10^5$ and $Pr = 344.7$ with bottom wall heated. It is worthy to note that both the effects of temperature dependence of viscosity and buoyancy are involved in this heating condition. It is shown that the deviations of Nu at each axial position are all less than 1%. Therefore, $M \times N = 60 \times 60$ and $\Delta z = 5 \times 10^{-6}$ are used in the present computation.

Only the data of Ra_q, Re, Pr and Gr_q/Re^2 are shown in Xie and Hartnett [1], but the values of Q in equation (2) are required in the present numerical study. To obtain the values of $Q = b(q_w D_h/k)$ from the available data, the value of $b = 0.0396$ is first obtained by a curve fitting to the viscosity data of mineral oil and the results is shown in Fig. 2. The following equation is used to calculate $\theta_c (= q_w D_h/k)$.

$$Pr^2 Gr_q = (g\beta D_h^3/\alpha^2)(q_w D_h/k). \quad (12)$$

One may ask why we did not calculate θ_c directly from the data of Ra_q or Gr_q. It is worthy to note that the value of v in Ra_q or Gr_q in equation (3) is rather temperature sensitive, therefore the corresponding values of θ_c in the experimental work of Xie and Hartnett [1] are hard to obtained directly from the data of Gr_q or Ra_q. But the value of α is relatively temperature insensitive, and θ_c can be obtained from the equation (12). The values of Q and the corresponding parameters of Ra_q, Gr_q/Re^2, Re and Pr for the three heating conditions are shown in Tables 2(a)–(c).

The results are basically divided into three parts. Part one including Figs. 3–5 is for the case of top wall heated. In the second part, Figs. 6–8 are for the case of bottom wall heated. The results for the case of both top and bottom walls heated are shown in Figs. 9 and 10.

The axial development of velocity distributions $w = (W/W_0)$ along y at the symmetry plane ($x = 0.75$) are shown in Fig. 3 for $Q = 24.4$, $Ra_q = 27.8 \times 10^5$ and $Pr = 318$. It is seen that the velocity distribution is quite symmetric at $z = 0.0005$. But as z increases, the velocity distributions are no longer symmetrical and the velocity profiles are more and more distorted toward the heated top wall. It is mainly due to the temperature dependence of viscosity. It is worthy to note in Fig. 3 that the rate of velocity distortion is larger in the region near the thermal entrance, such as z from 0.0005 to 0.005, than that near the fully developed region, such as z from 0.015 to 0.025.

The distortion of axial velocity will induce sec-

Table 1. Numerical experiments on the mesh system $M \times N$ and the axial step size Δz for the case of $Q = 18.72$, $Ra_q = 19.7 \times 10^5$ and $Pr = 344.7$ with bottom wall heated

$M \times N$ (Δz)	*Nu*			
	z			
	0.005	0.010	0.020	0.025
48×48 (0.000005)	12.96632	15.18570	17.27563	17.43950
60×60 (0.000005)	12.99082	14.87436	17.32186	17.49870
80×80 (0.000005)	13.01733	14.85850	17.34065	17.50419
60×60 (0.000002)	12.96788	14.87478	17.32258	17.50826

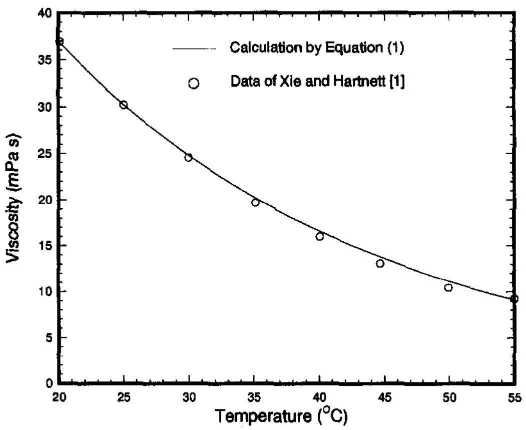

Fig. 2. Theoretical computation and experimental data for the temperature-dependent viscosity of mineral oil.

ondary flow. The axial development of secondary flow for $Q = 24.4$, $Ra_q = 27.8 \times 10^5$ and $Pr = 318$ is shown in Figs. 4(a)–(d). It is seen in Fig. 4 that the secondary flow is stronger at $z = 0.0025$ and $z = 0.005$ than that at $z = 0.03$. The motions of secondary flow at $z = 0.0025$ and 0.005 are mainly upward, but there are both upward and downward motions for secondary flow at $z = 0.01$ and 0.03. The strong upward secondary flow at $z = 0.0025$ and 0.005 is mainly caused by the larger rate of change (axial gradient) of velocity distortion, i.e. $\partial w/\partial z$, at the region near the thermal entrance as what we discussed in Fig. 3. But along with the increase of axial distance z, the rate of velocity distortion approaches an asymptotic smaller constant, and the secondary flow becomes weaker. It is also worthy to note that though there is secondary flow induced by the axial velocity distortion, the magnitude of secondary flow $(u^2+v^2)^{1/2} = (U^2+V^2)^{1/2}/(W_0 Gr_q/Re)$ is still much smaller than that of main flow. It is noted that the scale of the typical vector represented in Fig. 3 is for $(u^2+v^2)^{1/2} = 1.67 \times 10^{-5}$.

The variations of local Nusselt number *Nu* with *z* are shown in Fig. 5. It is seen that the present numerical results agree with the experimental data of Xie and Hartnett [1]. It is also seen that the curves of *Nu* with higher *Q* fall above those with lower *Q*. And a monotonically decrease of *Nu* with the increase of *z* is seen in each curve due to the thermal entrance effect. It is found that the axial velocity distortion due to temperature dependence of viscosity has a much larger contribution in the heat transfer enhancement than the effect of secondary flow.

The second part of the present results is for the case of bottom wall heated. The axial development of velocity distributions *w* along *y* at the symmetry plane is shown in Fig. 6 for $Q = 18.72$, $Ra_q = 19.7 \times 10^5$ and $Pr = 344.7$. It is seen that the velocity distribution is quite symmetric for $z = 0.0005$. As z increases to 0.005, the velocity profile is distorted toward the heated bottom wall. It is mainly due to the temperature dependence of viscosity. This axial velocity distortion is similar to that occurred in the case of top wall heated. But as z further increases to 0.01 and 0.025, the velocity profiles are more and more distorted away from the bottom heated wall. It is mainly due to the effect of buoyancy-induced secondary flow. The mixing mechanism caused by the buoyancy-induced secondary flow will smooth out the temperature distribution. Therefore the velocity distortion caused by the temperature dependence of viscosity is somewhat counterbalanced by the buoyancy-induced secondary flow. It is worthy to note that this counterbalance in velocity distortion, which occurred at larger z, is quite different from that shown in the cases of top wall heated.

To see how the combined effect of buoyancy and temperature-dependent viscosity influences the development of secondary flow is very useful to clarify the mechanism of heat transfer enhancement. The axial development of secondary flow is shown in Fig. 7 for $Q = 18.72$, $Ra_q = 19.7 \times 10^5$ and $Pr = 344.7$. It is seen that the secondary flow pattern is made up of a single eddy only at $z = 0.0025$, and the strength of the eddy is relatively weak. The strength of secondary flow significantly increases when z increases to 0.005. A second eddy arises at $z = 0.01$ in the central lower region of the channel. It is caused by the adverse temperature gradient in the vertical direction occurred

Table 2. Data of Ra_q, Gr_q, Re and Pr in the experimental work of Xie and Hartnett [1] and the corresponding values of Q for the cases of (a) top wall heated, (b) bottom wall heated and (c) both top and bottom wall heated

(a)

$10^{-6}Ra_q$	Gr_q/Re^2	Re	Pr	Q
0.48	0.447	55.8	341.4	4.45
0.58	0.112	120.6	354.5	5.62
0.88	0.0274	308.7	335.2	8.05
2.78	0.0174	709.0	318.8	24.41
1.74	0.0046	1003.3	374.9	17.87
1.72	0.0027	1300.1	375.4	17.65

(b)

$10^{-6}Ra_q$	Gr_q/Re^2	Re	Pr	Q
0.12	0.0061	220.1	407.2	1.50
0.47	0.4500	55.6	342.4	4.45
0.86	0.0306	284.7	346.1	8.05
1.73	0.0047	983.1	380.9	17.87
1.97	0.0146	627.0	344.7	18.72

(c)

$10^{-6}Ra_q$	Gr_q/Re^2	Re	Pr	Q
0.132	0.335	36.2	316.5	1.2
1.29	0.0265	512.6	278.5	13.76
2.21	0.0092	950.8	265.5	15.23
1.79	0.0023	1534.5	332.2	15.53

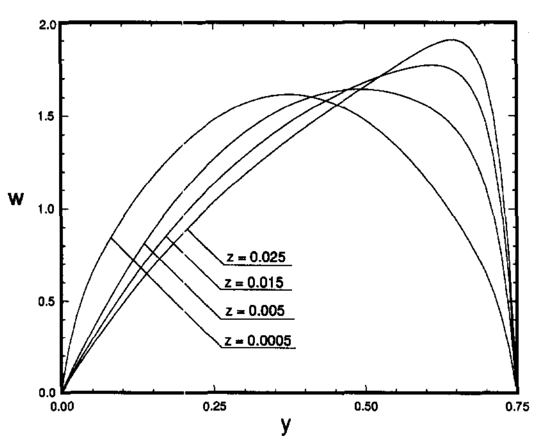

Fig. 3. Development of dimensionless axial velocity w along dimensionless coordinate y at the symmetry plane for $Q = 24.4$, $Ra_q = 27.8 \times 10^5$ and $Pr = 318$ with top wall heated.

in the region near the center of bottom heated wall. Along with the buildup of the adverse temperature gradient, the second eddy becomes stronger at $z = 0.03$. It is also noted in Fig. 7 that the scale of the reference vector represented in the Fig. 3 is for $(u^2+v^2)^{1/2} = 1.67 \times 10^{-4}$. Since under a fixed z, there is no significant difference in the values of Pr, Gr_q and Re between the cases shown in Figs. 4 and 7. Compared with that already shown in Fig. 4, it is seen that the strength of secondary flow shown in Fig. 7 at $z = 0.03$ for bottom wall heated is almost 20 times larger than that at $z = 0.03$ for top wall heated.

The variations of local Nusselt number Nu with z are shown in Fig. 8. for $Q = 18.72$, $Ra_q = 19.7 \times 10^5$ and $Pr = 344.7$. It is seen that the present numerical results are again in good agreement with the experimental data of Xie and Hartnett [1]. It is also seen that the curves of Nu with higher Q fall above those with lower Q. A monotonic decrease of Nu with the increase of z is seen in each curve for $z < 10^{-3}$ due to the thermal entrance effect. But as $z > 2 \times 10^{-2}$, the results of Nu for bottom wall heated are quite different from those for top-wall heated. Since the heat transfer enhancement due to buoyancy-induced secondary flow increases gradually, a minimum local Nusselt number occurs due to the combined thermal entrance and buoyancy effects. It is found that the axial velocity distortion due to temperature dependence of viscosity has a stronger contribution to the heat transfer enhancement than the buoyancy-induced secondary flow for lower z. While for higher z, the heat transfer enhancement is mainly caused by the buoyancy-induced secondary flow.

The third part of the present results is for the cases of both top and bottom walls heated. The axial development of velocity distribution w along y at the symmetry plane is shown in Fig. 9 for $Q = 13.76$, $Ra_q = 12.9 \times 10^5$ and $Pr = 275.8$. It is seen that the

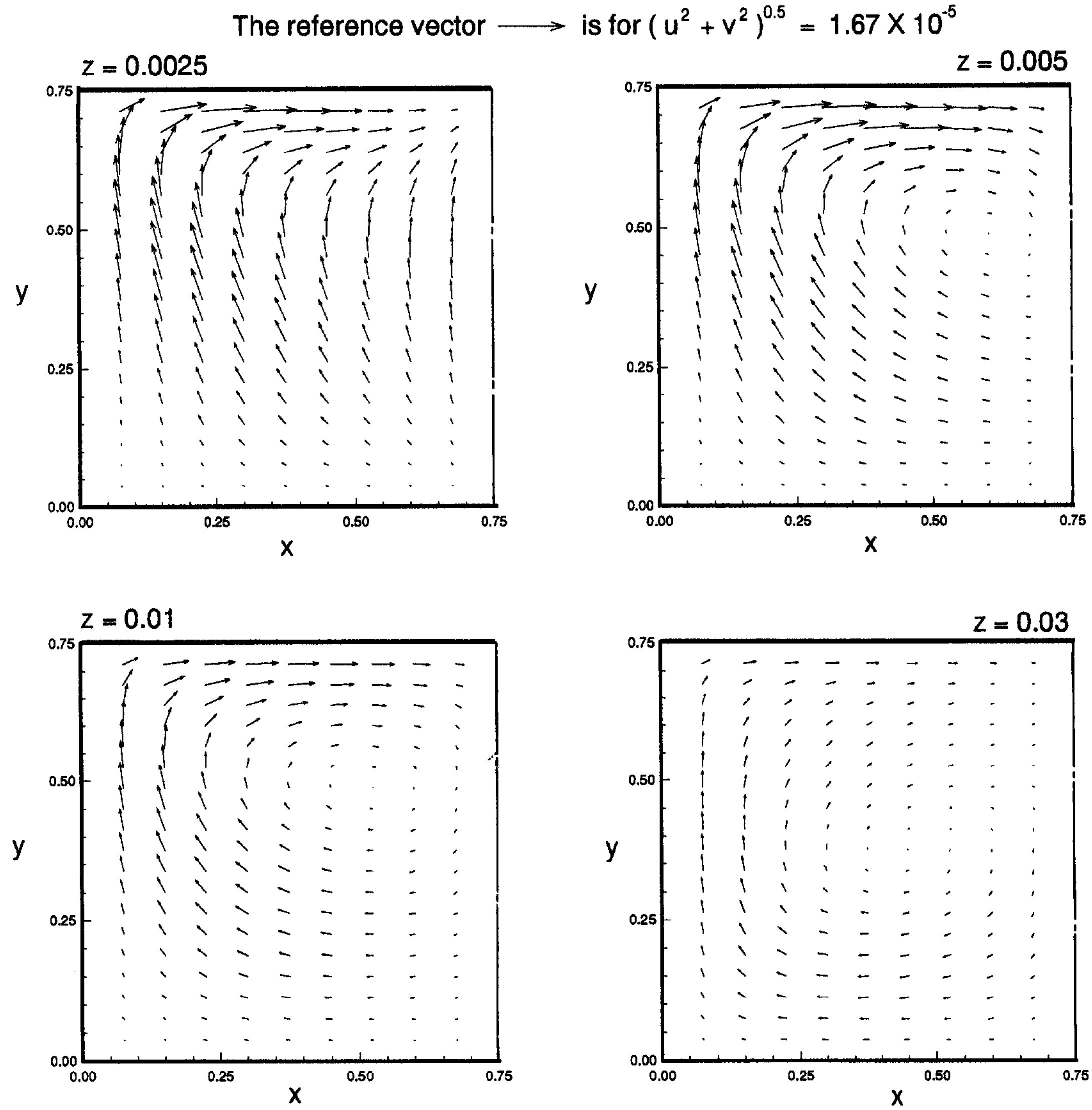

Fig. 4. Development of secondary flow for $Q = 24.4$, $Ra_q = 27.8 \times 10^5$ and $Pr = 318$ with top wall heated.

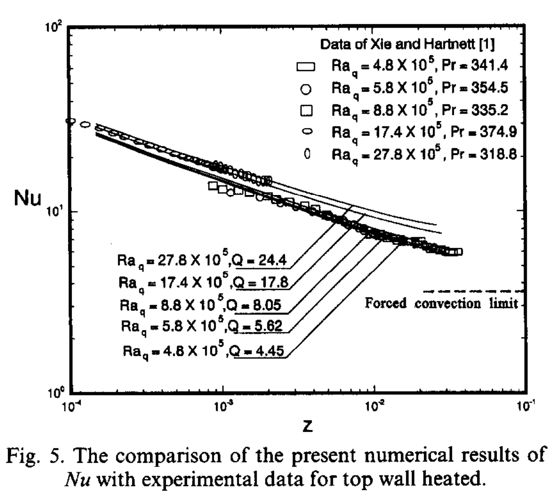

Fig. 5. The comparison of the present numerical results of Nu with experimental data for top wall heated.

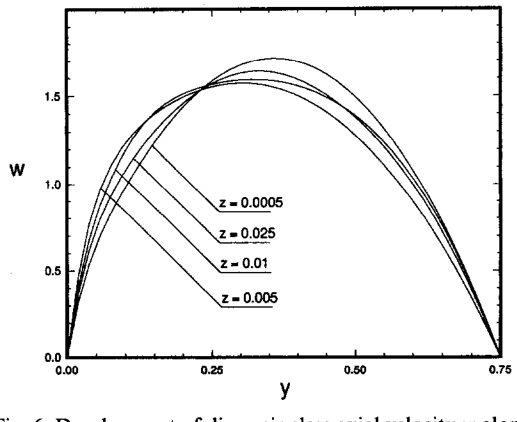

Fig. 6. Development of dimensionless axial velocity w along dimensionless coordinate y at the symmetry plane for $Q = 18.72$, $Ra_q = 19.7 \times 10^5$ and $Pr = 344.7$ with bottom wall heated.

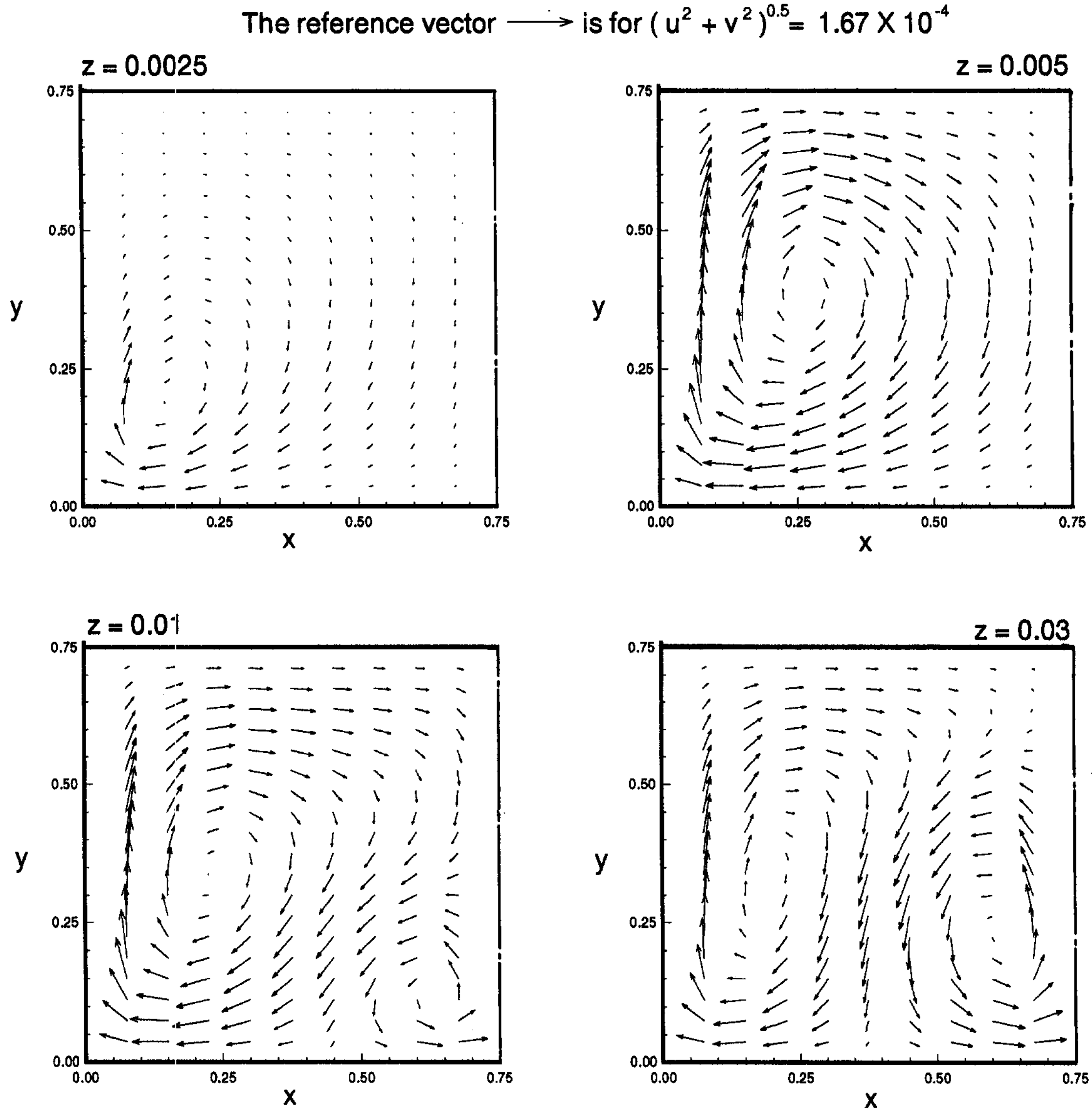

Fig. 7. Development of secondary flow for $Q = 18.72$, $Ra_q = 19.7 \times 10^5$ and $Pr = 344.7$ with bottom wall heated.

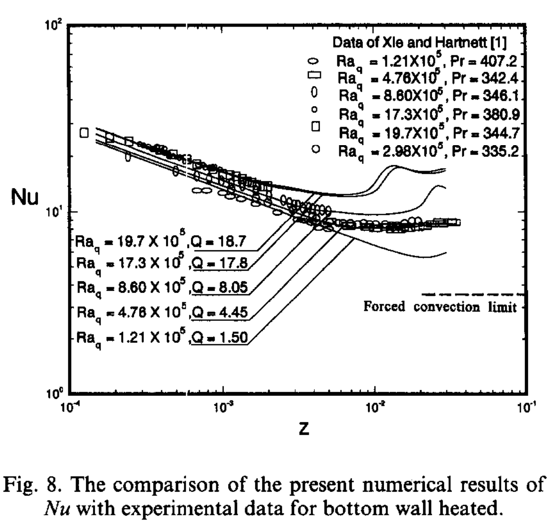

Fig. 8. The comparison of the present numerical results of *Nu* with experimental data for bottom wall heated.

velocity distribution is quite symmetric for $z = 0.0005$. As z increases to 0.005, the velocity profile is still quite symmetric, but becomes more uniform. The magnitude of the peak velocity decreases, and the velocity at the regions near both the heated top and bottom walls increases. It is mainly due to the temperature dependence of viscosity. As z further increases to 0.015 to 0.03, the peak of velocity moves toward the top heated wall. It is mainly due to the effect of the buoyancy-induced secondary flow. Since the hotter fluids move upward due to buoyancy effect, even both the top and bottom walls are heated with the same heat flux, the top wall becomes hotter and hotter than the bottom wall.

The variations of local Nusselt number Nu with z are shown in Fig. 10. for $Q = 13.76$, $Ra_q = 12.9 \times 10^5$ and $Pr = 275.8$. The value of Nu in Fig. 10 is an

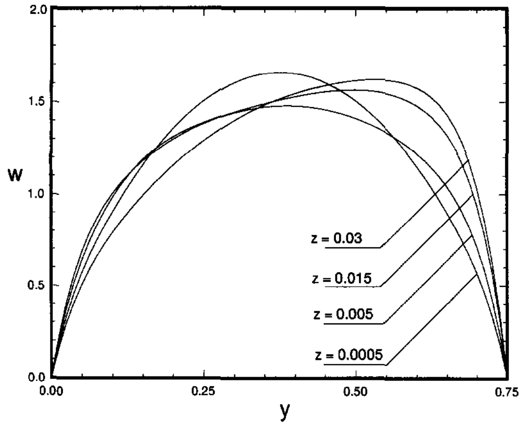

Fig. 9. Development of dimensionless axial velocity w along dimensionless coordinate y at the symmetry plane for $Q = 13.76$, $Ra_q = 12.9 \times 10^5$ and $Pr = 275.8$ with both top and bottom walls heated.

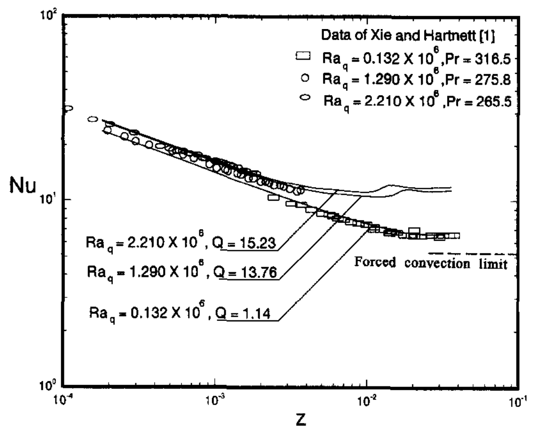

Fig. 10. The comparison of the present numerical results of Nu with experimental data for both top and bottom walls heated.

average value of Nu for the top and bottom walls. It is seen that the present numerical results are again in good agreement with the experimental data of Xie and Hartnett [1]. It is also seen that the trend of Nu curve for both top and bottom walls heated is more like that for bottom wall heated rather than that for top wall heated.

CONCLUDING REMARKS

A numerical study is performed to study the mechanism of heat transfer enhancement for mineral oil in 2 : 1 rectangular ducts. Three different heating conditions are considered: top wall heated, bottom wall heated, and both top and bottom walls heated. For the three heating conditions, the present numerical results are all in good agreement with the experimental data of Xie and Hartnett [1]. The key findings are as follows:

(1) For the case of top wall heated, the axial velocity profile is distorted toward the heated top plate due to the effect of temperature dependence of viscosity. The distortion of axial velocity will induce secondary flow. But the heat transfer enhancement is caused mainly by the effect of axial velocity distortion, and the effect of distortion-induced secondary flow is rather minor.

(2) For the case of bottom wall heated, secondary flow is caused both by the distortion of axial velocity and buoyancy effect. In the region near the entrance, i.e. for lower z, the axial velocity distortion due to temperature dependence of viscosity has a stronger contribution to the heat transfer enhancement than the buoyancy-induced secondary flow. While for higher z, the heat transfer enhancement is mainly caused by the buoyancy-induced secondary flow.

(3) By the comparison between the cases of top wall heated and bottom wall heated shown in Figs. 4 and 7 under the same order of Ra_q and Pr, it is worthy to note that the strength of buoyancy-induced secondary flow is almost 20 times larger than that of distortion-induced secondary flow at $z = 0.03$.

(4) The mechanism of heat transfer enhancement in the duct with both top and bottom walls heated is more like that for bottom wall heated rather than that for top wall heated.

Acknowledgement—Financial support from the National Science Council of Republic of China through Project NSC 83-0401-E008-053 is greatly appreciated.

REFERENCES

1. C. Xie and J. P. Hartnett, Influence of variable viscosity of mineral oil on laminar heat transfer in a 2 : 1 rectangular duct, *Int. J. Heat Mass Transfer* **35,** 641–648 (1992).
2. J. P. Hartnett, Viscoelastic fluids: a new challenge in heat transfer, *J. Heat Transfer* **114,** 296–303 (1992).
3. C. Xie and J. P. Hartnett, Influence of rheology on laminar heat transfer to viscoelastic fluids in a rectangular channel, *Ind. Engng Chem. Res.* **31,** 727–732 (1992).
4. J. P. Hartnett and M. Kostic, Heat transfer to a viscoelastic fluid in laminar flow through a rectangular channel, *Int. J. Heat Mass Transfer* **28,** 1147–1155 (1985).
5. E. N. Sieder and G. E. Tate, Heat transfer and pressure drop of liquids in tubes, *Ind. Engng Chem.* **23,** 1429–1435 (1936).
6. R. G. Deissler, Analytical investigation of fully developed laminar flow in tubes with heat transfer with fluid properties variable along the radius, NACA TN 2410, Washington (July 1951).
7. K. T. Yang, Laminar forced convection of liquids in tubes with variable viscosity, *J. Heat Transfer* **84,** 353–362 (1962).
8. R. L. Shannon and C. A. Depew, Forced laminar flow convection in a horizontal tube with variable viscosity and free convection effects, *J. Heat Transfer* **91,** 251–258 (1969).
9. F. L. Test, Laminar flow heat transfer and fluid flow for liquids with temperature-dependent viscosity, *J. Heat Transfer* **90,** 385–393 (1968).

10. S. Hong and A. E. Bergles, Theoretical solutions for combined forced and free convection in horizontal tubes with temperature-dependent viscosity, *J. Heat Transfer* **98,** 459–465 (1976).
11. R. Oskay and S. Kakac, Effect of viscosity variations on forced convection heat transfer in pipe flow, *METU J. Pure Appl. Sci.* **6,** 211–230 (1973).
12. H. W. Butler and D. E. Mckee, An exact solution for the flow of temperature-dependent viscous fluids in heated rectangular ducts, *J. Heat Transfer* **95,** 555–557 (1973).
13. S. Shin, Y. I. Cho, W. K. Gingrich and W. Shyy, Numerical study of laminar heat transfer with temperature-dependent viscosity in a 2:1 rectangular duct, *Int. J. Heat Mass Transfer* **36,** 4365–4373 (1993).
14. F. C. Chou, F. K. Tsou and C. W. Tung, Numerical studies of non-Newtonian channel flow and heat transfer enhancement for electronics modules, *Procs. of 1993 ASME Winter Annual Meeting*, New Orleans, Louisiana, ASME HTD-Vol. 263, Enhanced Cooling Techniques for Electronics Applications, pp. 89–98 (1993).
15. F. C. Chou and G. J. Hwang, Vorticity-velocity method for the Graetz problem and the effect of natural convection in a horizontal rectangular channel with uniform wall heat flux, *J. Heat Transfer* **109,** 704–710 (1987).